Fuel Processing Technology 193 (2019) 378–391

Contents lists available at ScienceDirect

Fuel Processing Technology

journal homepage: www.elsevier.com/locate/fuproc

Reforming of biogas using a non-thermal, gliding-arc, plasma in reverse vortex flow and fate of hydrogen sulfide contaminants

S.M. Ali Mousavi*, William Piavis, Scott Turn

Hawaii Natural Energy Institute, University of Hawaii, 1680 East-West Rd., POST 109, Honolulu, HI 96822, USA

ARTICLE INFO

Keywords:
Biogas
Non-thermal plasma reforming
Gliding arc plasma reforming
Methane
Hydrogen production
Sulfur

ABSTRACT

Biogas is being produced everyday around the world due to land filling of organic wastes. Reforming of biogas to hydrogen rich gas offers a green source of energy. This work demonstrates reforming biogas into hydrogen rich gas via a non-thermal gliding arc plasma stabilized in a reverse vortex flow with very low and competitive specific energy requirement. Parametric tests determined the individual effects of power input (140-300 W), steam to carbon ratio (0.0–3.0), and equivalence ratio (0.1–0.7) on reformer performance. Factorial tests identified optimal operating condition based on minimizing the specific energy requirement, determined to be 184 kJ/mol H_2 or 1.91 eV/H_2 molecule, significantly below the value for conventional steam reforming of methane, 3.37 eV/H_2 molecule produced. The optimum operating conditions were found at an equivalence ratio of 0.11, a steam to carbon ratio of 0.14, and an input plasma power of 160 W, resulting in methane conversion of 48.8%, hydrogen yield of 23.4%, hydrogen selectivity of 47.8%, and an efficiency of 25.3%. Hydrogen sulfide as a common contaminant in landfill gas has detrimental effects on downstream facilities. The reactor was also evaluated on synthetic biogas containing hydrogen sulfide at low concentration (21 ppm). About 5.7% of the sulfur input to the system was partitioned to the dry outlet reformate stream with the remainder captured as sulfate in a downstream impinger or recovered as a solid of unknown molecular structure deposited on tubing surfaces between the reformer and the impinger. This reforming technology offers potential to be deployed as a lightweight compact portable system for on-site applications such as landfills, and depending on available fuels, in mobile applications such as ships.

1. Introduction

The field of alternative energy production is growing in response to climate change awareness, fossil fuel costs, and energy security concerns. Accessible, environmentally friendly, sustainable, secure sources of energy that can meet projected energy requirements are needed [1]. Hydrogen is expected to play a larger role in the future energy portfolio [2,3]. Among different sources and methods of hydrogen production, plasma assisted reforming of hydrocarbons shows promising results [4–9].

Biogas from landfills contains 40 to 60% methane with the balance being largely carbon dioxide. < 2% of the biogas is typically nitrogen, oxygen and other trace volatile organic compounds (VOCs) [10]. Because methane is 20 to 25 times more potent a greenhouse gas (GHG) than CO_2, decomposing municipal solid waste can be a serious climate change contributor. The U.S. EPA predicts global biogas emissions will grow by 13% between 2010 and 2030 [11]. Sulfate reducing microorganisms produce hydrogen sulfide in landfills. H_2S is hazardous due to its effects on both humans and materials, corroding metal components in pipelines, sensors, engines, etc., and poisoning catalysts in fuel cell applications [12]. For proton exchange membrane (PEM) fuel cell road vehicles [13], the International Organization for Standardization (ISO) dictates a limit of 0.004 μmol total sulfur compounds (as H_2S) per mole of H_2 at the dispenser nozzle [14,15]. Thus, practical use of biogas as hydrogen feedstock depends on economical removal of H_2S to meet these limits. Converting H_2S into easily removed sulfur forms may enhance removal between the reformer and the fuel cell. This paper explores reforming of simulated biogas, a nominally 50:50 mixture of methane (a renewable hydrocarbon) and carbon dioxide, in a non-thermal gliding arc plasma reactor stabilized in a reverse vortex flow (RVF). Operating conditions that minimize the specific energy ratio (defined as the energy input as power to the arc divided by the number of moles of hydrogen produced) were identified using response surface methodology. The fate of hydrogen sulfide at contaminant concentrations in the simulated biogas is also explored to identify operating conditions that minimize sulfur concentration in the dry biogas reformate.

* Corresponding author at: Department of Mechanical Engineering, Virginia Tech, 460 Old Turner St., Blacksburg, VA 24061, USA.
E-mail addresses: mousavi@hawaii.edu (S.M.A. Mousavi), sturn@hawaii.edu (S. Turn).

https://doi.org/10.1016/j.fuproc.2019.05.031
Received 6 February 2019; Received in revised form 24 April 2019; Accepted 21 May 2019
Available online 04 June 2019
0378-3820/ Published by Elsevier B.V.

1.1. Hydrocarbon reforming technologies

Reforming uses carbon sources (gas, liquid, solid) to produce hydrogen with general goals of maximizing hydrogen production while minimizing carbon monoxide production, although several other process performance indicators may be appropriate as will be discussed later. Partial oxidization (POX), auto-thermal reforming, and steam reforming (SR) [16] are three primary industrial fuel reforming techniques [17]. Eqs. (1) and (2) describe general methane reforming and ideal methane steam reforming, respectively. The latter is endothermic and typically occupies a large system footprint, experiences thermal lag, and requires expensive catalysts.

$$CH_4 + nH_2O + mO_2 \rightarrow xCO + yCO_2 + cH_2O + dH_2 + eCH_4... \quad (1)$$

$$CH_4 + 2H_2O \rightarrow CO_2 + 4H_2 \qquad (\Delta H = 165\ kJ/mol) \quad (2)$$

POX (Eq. (3)) and auto-thermal reforming are both exothermic, oxidizing a fraction of the fuel stream to propagate the reforming reactions. Auto-thermal reforming, a combination of steam reforming and POX [17], requires specific reactant ratios and high temperatures. It is prone to coking, catalyst deactivation [18], and slowly responds to system changes making it impractical for mobile applications [5,19].

$$CH_4 + 0.5O_2 \rightarrow CO + 2H_2 \qquad (\Delta H = -36\ kJ/mol) \quad (3)$$

Since the 1990's, plasma reforming technologies have been employed to reform diesel, renewable diesel [20,21], methane [3–5,7–9,20,22], ethanol [20], isooctane [8,22], toluene [23] and gasoline [24]. Advantages of plasma reformers include reduced system cost, reduced catalyst deterioration (if a catalyst is employed), a smaller footprint, rapid response time, and the ability to reform heavy hydrocarbons [5,17,24–27]. Plasma reformers can also be configured to operate at near ambient temperatures [26,28,29]. Electrode erosion at high temperature and electricity input requirements are potential disadvantages.

Plasmas generally falls into one of two categories - thermal or non-thermal. In a thermal plasma, gas molecules and electrons exist in thermal equilibrium. Scales range from 1 kW to over 50 MW [20,26] and create temperatures ranging from 5000 to 10,000 K. At these high temperatures, the electrodes must be cooled to reduce thermal erosion [20].The gas molecules and electrons in non-thermal plasma are not in thermal equilibrium. The gas molecules can exist at near-ambient temperature, while the electrons are excited at 10,000 to 100,000 K (1–10 eV) [19]. Non-thermal plasma reformers require electrical energy on the order of 10^2 W, have low electrode erosion, avoid the need for a cooling system, occupy a small footprint, and are low weight [20]. For similar hydrogen yields, non-thermal plasma reformers require less energy input, when compared to their thermal counterparts [6].

Pornmai et al. [30] studied plasma reforming of a 70:5:5:20 mixture of CH_4:C_2H_6:C_2H_8:CO_2 using reactant steam. The gliding arc reactor was fed with 100 cm^3/min of "simulated natural gas" with O_2 added to produce a hydrocarbon to O_2 molar ratio of 2:1 and 10% molar steam. The energy cost was reported to be 7.62 eV/H_2 molecule produced. Chun et al. [31] used a gliding arc reactor that was equipped with three fan-shaped electrodes located 120° apart. An external gas burner kept the plasma reactor at 580 °C followed by a catalyst reformer at 700 °C. The optimum working condition, reported at a steam to carbon ratio (SCR) of 3.0, had a SER value of 3.00 eV/H_2 molecule produced with 100% CH_4 conversion and 59% H_2 selectivity. It should be noted that the energy spent preheating the plasma and catalyst reformer was not considered. In a study done with a gliding arc reactor in co-axial electrode configuration, Li et al. reported that the heat insulated reactor equipped with Ni-based catalyst running on biogas has an advantage of auto-reduction of the catalyst during start up. The inlet gas molar ratio was CH_4:CO_2:O_2 = 3:2:1.8 and SER of 48 kJ/mol H_2 (without catalyst) and 17 kJ/mol H_2 (with catalyst), and energy efficiency of 50% (without catalyst) and 86%(with catalyst) were achieved [32].

1.2. Plasma reforming of hydrogen sulfide

Elemental sulfur and its compounds have application in different sectors, such as food, agriculture, energy and power production [33,34]. The Claus process is a conventional method for recovering elemental S from H_2S. In this process, H_2S is converted to elemental sulfur (S) and water (H_2O) via a two-step reaction shown in Eqs. (4) and (5) [35].

$$H_2S + 1.5O_2 \rightarrow SO_2 + H_2O \text{ (thermal step)} \quad (4)$$

$$SO_2 + 2H_2S \rightarrow 3S + 2H_2O \text{ (catalytic and thermal step)} \quad (5)$$

Direct decomposition of H_2S into H_2 and S, shown in Eq. (6) can also extract S from H_2S.

$$H_2S \rightarrow H_2 + \frac{1}{2}S_2 \qquad \Delta H_r = 20.4\ kJ/mol \qquad \Delta G = 33.3\ kJ/mol \quad (6)$$

Positive changes in enthalpy and Gibbs free energy across Eq. (5) indicate an endothermic and non-spontaneous reaction. For example, only 12% conversion of H_2S occurs at 1000 °C and 1 atm pressure, while below 550 °C < 1% conversion takes place [36]. Recent thermodynamic calculations at 1250 K by Nunnally et al. indicate that an energy input of 4 eV/H_2 molecule (386 kJ/mol-H_2) results in < 20% H_2S conversion [37]. An in-depth review by Luinstra concluded that the relatively low energy requirement of thermal and plasma methods makes them promising compared to electrochemical and photochemical methods [38,39]. Only Eq. (4) appears favored for contaminant levels of H_2S (~100 ppmv) in biogas from landfills undergoing plasma reforming.

Various non-thermal plasma systems have been studied for disassociation of H_2S, including dielectric barrier discharge, rotating glow, pulsed corona discharge, microwave discharge, gliding arc discharge, and radio frequency discharge [36,40–43]. Early stage technology for H_2S disassociation to form H_2 required roughly 500 eV/H_2 molecule produced [44,45]. Nunnally et al. [37] enhanced the flat gliding arc geometry with the gliding arc in tornado (GAT) and greatly reduced energy requirements to 1.2 eV/H_2 molecule produced. The decrease in energy requirement stems from increased gas contact with the plasma in a GAT system and the associated improvement in energy transfer. The result, 25% H_2S conversion to H_2, was produced at atmospheric pressure, a pure H_2S gas flow rate of 14 slpm, specific energy input of 0.31 eV/H_2S molecule, and ~240 W power input to the system. Using the same GAT system, 2.8 slpm O_2 was added to the 14 slpm H_2S flow, achieving a specific energy value of 1.0 eV/H_2 molecule produced [46].

1.3. Gliding arc tornado (GAT), reverse vortex non-thermal plasma

Biogas reforming using methods such as microwave discharge [47], plasma shade [48], and AC-pulsed gliding arc discharge have been studied [18,30,31,47,49]. Stabilization of gliding arc plasma within a reverse vortex flow has shown encouraging results [4,50].

Gliding arcs and forward vortex reactor chambers [18,31,32] have been used to reform biogas. Fig. 1(a) shows schematic of conventional gliding arc where the arc propagates in the Z direction and move upward with time. Fig. 1(b) depicts a 3D schematic of the gliding arc reverse vortex flow plasma used in this study. A stable gliding arc ignites between the top and bottom electrode and propagates by rotating around the Z axis. The reverse vortex increases the residence time of the reactant within the plasma arc and produces a more uniform gas treatment than conventional gliding arcs [51]. Gases swirling along the reactor wall produce near-perfect thermal insulation, and the movement of the arc reduces thermal erosion and eliminates the necessity to fabricate the reaction chamber from materials with high-temperature tolerance [51]. Forward vortex reactors have the same tangential gas injection at one end of the cylindrical reaction chamber, but with an axial exit at the opposite end.

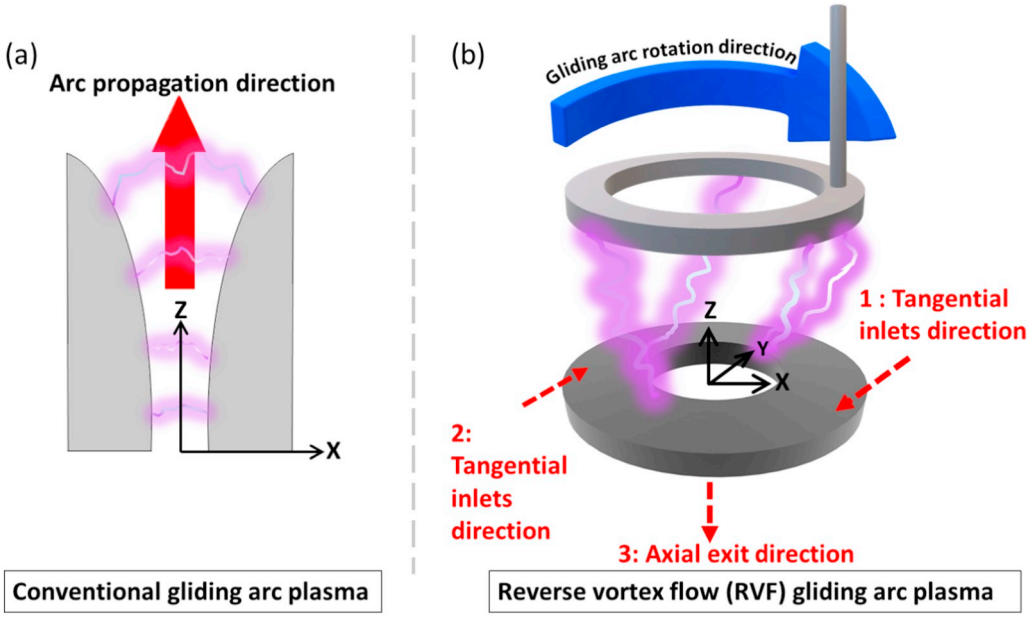

Fig. 1. Schematic of gliding arc systems. (a): Conventional 2D gliding arc plasma. (b): Reverse vortex flow gliding arc plasma used in this study.

This report uses the reverse vortex flow reactor to reform simulated landfill biogas. Unlike the work by Pornmai et al. [30] and Chun et al. [31], the present study explores direct reforming of the biogas without additional catalyst or additional energy consumption for heating the plasma reformer. The reverse vortex flow reactor advantages of increased contact between the reactants and the arc and better thermal management are apparent in the experimental results. Reforming gases with different CH_4:CO_2 ratios have yielded promising results in other types of reactors, however information on reforming biogas by reverse vortex flow reactor and also the fate of contaminants is severely lacking. This study seeks to address this information gap, by adding hydrogen sulfide to biogas reformed in the partial oxidative environment of the reverse vortex flow gliding arc reactor.

2. Materials and methods

This section describes the testbed, sample characterization in different states of solid, gaseous and liquid, system parameters, parametric tests, and the factorial experimental design utilized in system optimization. Fig. 2 shows the reforming testbed used for biogas and sulfur management in this study.

2.1. Testbed modifications

Reactant delivery, reformer, reformate conditioning, and analysis modifications were made prior to conducting experiments with simulated biogas containing 0 to 45 ppm of H_2S. To prevent sulfur loss by adsorption, all the wetted surfaces exposed to fuel and reformate were converted to sulfur inert materials, i.e. metals subjected to the SilcoNert® process (SilcoTek, Bellefonte, PA, USA), ceramics, or polytetrafluoroethylene (PTFE).

The reactant delivery system is shown in rectangle-A of Fig. 2. It consists of nitrogen and oxygen compressed gas cylinders and mass flow controllers (Brooks 5850E, USA) controlled by LabView running on a computer. Steam was generated by metering deionized water (Eldex 38 M 1/800 piston pump) to a heated section of delivery tube immediately upstream of the reactor. A permeation tube device (Model 491, KIN-TEK Laboratories, Inc., La Marque, TX USA) was used to meter 0 to 45 ppm of H_2S into a premixed, synthetic biogas (50%–50% methane-carbon dioxide) stream that entered the reformer via the tangential-inlet zirconia plate. PTFE tubing was used between the Kin-Tek and the reformer. A 3 mm PTFE line bypassed the reformer to allow calibration of gas analysis equipment directly from the reactant delivery system.

The reformate conditioning system is shown in rectangle-B of Fig. 2. Sulfur containing reformate passed through two glass impingers in series. The first impinger contained 100 ml of isopropyl alcohol (A416 2-Propanol Certified ACS Plus, Fisher Scientific, Hanover Park, IL) and the second was empty. Both were immersed in an ice water bath. A 6 mm diameter, 53 cm long PTFE sleeve lined the first impinger from the base of the 3 way valve at the outlet of the reformer to the bottom of the impinger inlet tube. The PTFE sleeve collected any precipitated solids that plated onto the tubing and was removed for examination after each test.

Exiting the impinger train, the reformate passed through a coalescing filter to capture remaining aerosol liquids and a mass flow meter (Model FMA1820A-ST-N2-EPR, Omega Engineering Inc., Norwalk, CT) to measure dry gas flow rate. A pump (Model R271-FT-EA-1, Air Dimensions, Deerfield Beach, FL) pulled a slip stream of the reformate through the sample loops of two gas chromatographs (GC) in series. The GC's identified major gas species and sulfur compounds. The remainder of the gas stream was vented into a fume hood. The GCs and the pump are shown in Fig. 2 rectangle-C. The online gas analyzers (Oxymat, Calomat, and Ultramat), mass flow meters, and Horiba gas conditioner shown in the upper right of Fig. 2 were all sulfur incompatible and were only used in a bypass mode for transitioning between test points when sulfur was absent from the system.

The entire reactor system was housed in a plexiglass enclosure to isolate it from laboratory personnel. The enclosure was placed directly beneath a canopy hood to remove heat and fugitive emissions. Fig. 3 depicts a cross sectional image of the gliding arc reverse vortex flow reactor. A lead wire and inconel washer were embedded into the non-conducting zirconia (AmZirOx 86, Astro Met Zirconium Oxide, Cincinnati, OH) plate. The inconel washer served as the lower electrode and formed the axial exit orifice of the reactor. The end plate at the top of the reactor was a solid Macor (Corning Inc., Corning, NY) plate with an upper electrode access port. All electrode materials were treated with SilcoNert®.

2.2. Gaseous sample characterization

A GC (Model 2014, Shimadzu, Colombia, MD) equipped with a sulfur chemiluminescence detector (SCD) (Sievers-355) and a 60 m long capillary column (RestekTM Model Rtx®-1) with a 0.53 mm internal

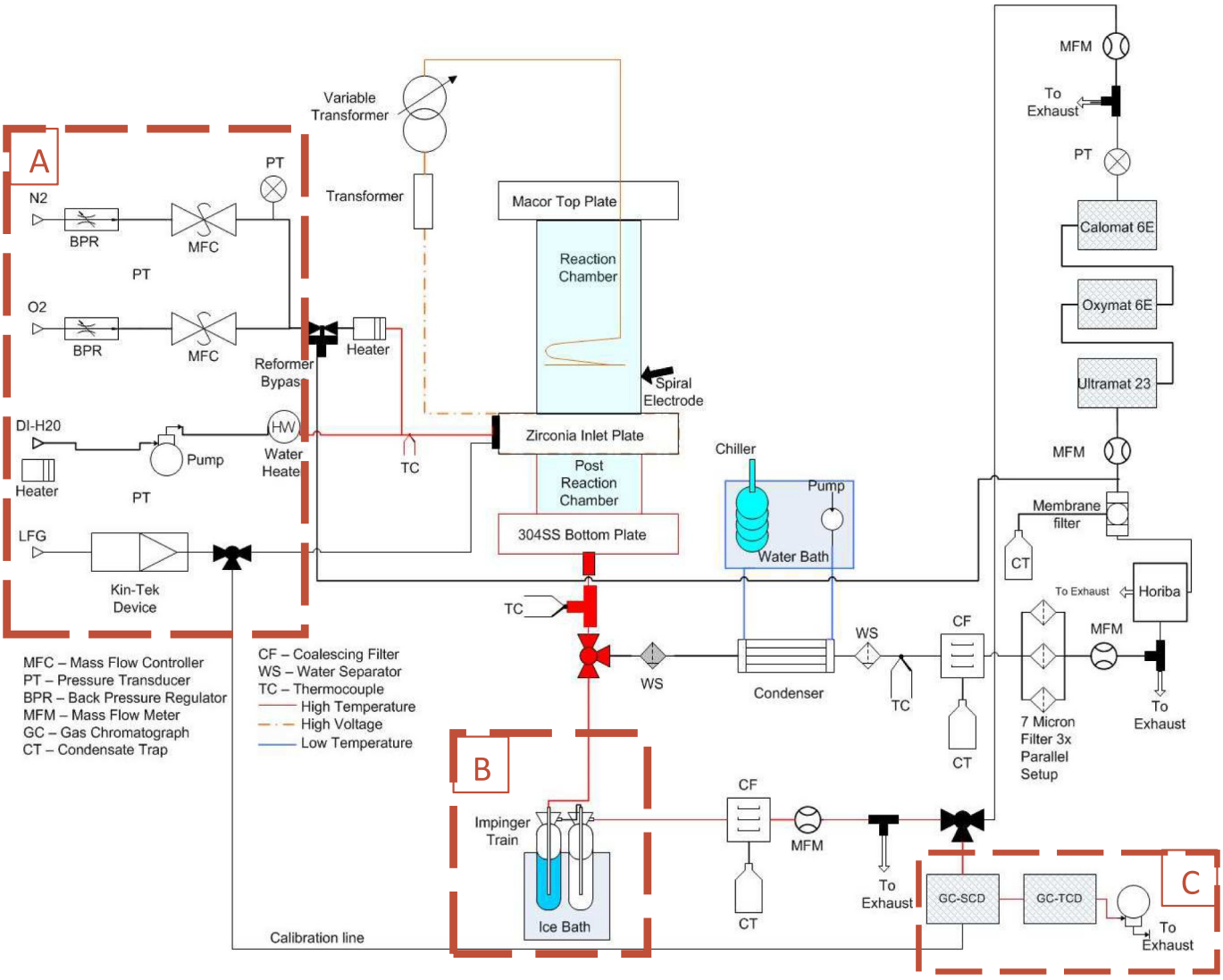

Fig. 2. Schematic diagram of the non-thermal plasma test bed. A: Reactant delivery section. B: Reformate conditioning system. C: Gas analyzers.

diameter, 7 μm stationary phase was used to quantify sulfur species. A second GC (Model 14A, Shimadzu, Columbia, MD) equipped with a thermal conductivity detector (TCD) and a 1.52 m × 3 mm Carboxen™ 1000 column (SUPELCO, Bellafonte, PA) quantified permanent gas species, N_2, CO, CO_2, H_2, and CH_4 in accordance with ASTM Standard D1946-90 – Standard Practice for Analysis of Reformed Gas by Gas Chromatography. Each set of reformer test conditions were maintained for 40 min with sampling occurring at 10 min intervals on both GCs.

2.3. Liquid sample characterization

Liquid samples collected from the impingers were analyzed for sulfur containing species with a dual Dionex ICS-1100 ion chromatograph (Thermo Fisher Scientific Inc., Waltham, Massachusetts, USA) with a conductivity detector. Anion analysis took place with a Dionex Ion Pac AS14A (4 mm × 250 mm) column, utilizing 8 mM Na_2CO_3 and 1 mM $NaHCO_3$ eluent at 1.0 mL/min with an AERS 500 suppressor at 43 mA. Anions were calibrated against Dionex 7 Anion-II. Cation analysis took place with a Dionex Ion Pac CS12A (4 mm × 250 mm) column, utilizing 20 mM methanesulfonic acid eluent at 1.0 mL/min with a CERS 500 suppressor at 59 mA. Cations were calibrated against Dionex 6 Cation-II. The pH was measured with an Accumet® Research AR25 Dual Channel pH/Ion Meter (Thermo Fisher Scientific Inc., Waltham, Massachusetts, USA).

2.4. Solid sample characterization

An analytical balance (model ME204E, Mettler-Toledo, Columbus, Ohio) was used to weigh the PTFE impinger liner before adding Swagelok hardware to the tube for connection to the system, post-test after hardware removal, and after 3 weeks of desiccation at 20–30% relative humidity. The mass gain of the tube resulted from solids collecting on the tube walls during tests. The tube was then halved lengthwise, sectioned into 10 pieces, and the dimensions and mass of each section were recorded. Adherent solids were removed from the tubing with a PTFE spatula and placed on a polished aluminum microscopy stub. A Hitachi S-4800 field emission scanning electron microscope (SEM) produced images of the sample on the stub at 25,000× magnification, at an acceleration voltage of 15 kV, and gun current of 20 μA. Energy dispersive spectrometer (EDS) spectra acquired with an Oxford INCA PentaFet-x3 Si(Li) EDS allowed for qualitative identification of solid species present in the sample.

2.5. System variables

System variables are categorized into dependent and independent variables in Table 1. Variable 1, the reactor chamber geometry affects the residence time of reactants within the reactor. The nonthermal plasma reactor used in these tests had a fixed geometry (42 mm ID,

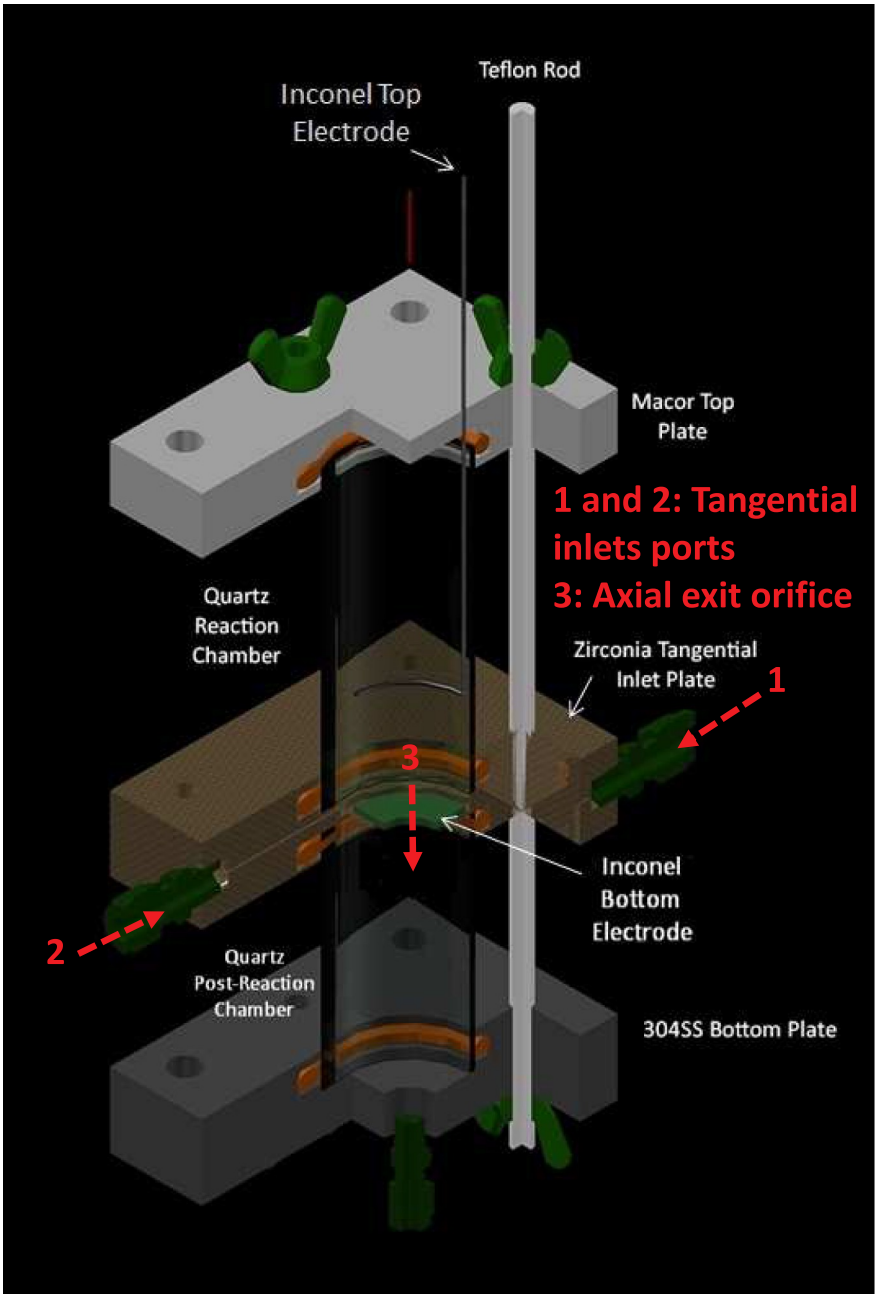

Fig. 3. Cross section of gliding arc reverse vortex flow non-thermal plasma reactor. (Silicon o-rings are orange color). The inlet 1 and 2 are tangential inlet ports of reactants. 3 is the axial exit orifice of reformates.

100 mm length, 0.138 l total volume). Variable 2, the post reactor chamber geometry, was fixed with an inner diameter of 42 mm, a length of 76 mm and a total volume of 0.105 l. The electrode gap distance, Variable 3, dictated the minimum power level necessary to sustain arc ignition and in these tests remained fixed at 25 mm.

Variable 4, Oxygen input, combined with fuel input, dictates the equivalence ratio (EQR) and the air fuel ratio (AFR), defined in Eq. (7).

$$EQR = \frac{AFR_{Reaction}}{AFR_{Stoichiometric}}, \text{ where } AFR = \frac{\dot{n}_{air}}{\dot{n}_{fuel}} \quad (7)$$

where $\dot{n}_{air}$ and $\dot{n}_{fuel}$ are the molar flow rates of air and fuel, respectively. In this reforming context, the value of EQR could range from 0 to 1.0, with EQR = 0 corresponding to no O_2 present in the reactant flow and EQR = 1.0 corresponding to the reactant ratio of O_2 to CH_4 equal to 2.0, that needed to completely convert CH4 to CO_2 and H_2O. Variable 5, nitrogen input, was another fixed independent variable. Nitrogen

Table 1
System variables.

#	Variable	Type
1	Reactor chamber	Independent [Fixed]
2	Post reaction chamber	Independent [Fixed]
3	Electrode gap distance	Independent [Fixed]
4	Oxygen input	Independent [Fixed]
5	Nitrogen input	Independent [Varied]
6	Biogas input	Independent [Varied]
7	Steam input	Independent [Varied]
8	Power input	Independent [Varied]
9	Reactor temperature	Dependent
10	Volumetric flow rate	Dependent

volumetric flow was set 3.77 times greater than oxygen in order to produce synthetic air,21% O_2 and 79% N_2. Premixed synthetic biogas, Variable 6, was metered from a compressed gas cylinder to the reactor system using a mass flow controller. The CH_4 component of the biogas was used in the AFR and EQR calculations. Variable 7, steam input to the system, was controlled by a precision metering pump and this independent variable was included in the steam to carbon ratio (SCR) calculation. Arc power (W), Variable 8, delivered by the power supply affects the number of electrons in the arc available for ionization of neutral particles. Note that power input was monitored but voltage and current were not. Variables 9 and 10 are dependent system variables. Power input level, reactant gas inputs, and electrodes gap distance (length of the arc) all affected reactor temperature. Inlet gas flow proportions were varied to produce the desired reactant gas ratios. The input flow and the reactor conditions dictated the reformate volumetric flow rate.

2.6. Experiment design and analysis methodology

In this section outlines testing methodologies. Initial parametric tests were followed by factorial tests. Reactor performance was then optimized using a central composite design method.

2.6.1. Parametric tests

Parametric testing focused on characterizing reactor performance changes as individual independent parameters were varied. Four independent experimental variables – equivalence ratio, steam to carbon ratio, plasma power, and sulfur input – were explored to determine their effects on system performance. The range of values for each independent variable and their base case values are shown in Table 2.

Combinations of variables that (1) either produced soot, (2) caused the plasma arc to behave erratically, or (3) produced conditions where the plasma arc could not form between the electrodes, defined operational system boundaries.

2.6.2. Factorial tests design

A 2^3 full factorial design, 8 points per test, exploring the effects of the independent variables EQR, SCR, and power input, were used to identify the system operating conditions that minimized the specific energy requirements (SER) (Eq. (8)).

$$\text{SER} = \frac{\text{Input Plasma Power}}{(\dot{n}_{CO} + \dot{n}_{H_2})_{\text{produced}}} (\text{kJ/mol}H_2 \text{ produced}) \quad (8)$$

where input plasma power is measured in kW, and $\dot{n}$ is molar flow rate in mol s^{-1}. Eq. (8) assumes that the water gas shift reaction shown in Eq. (9) can convert all CO present in the reformate to H_2. This assumption is also made for efficiency calculations.

$$H_2O + CO \rightarrow H_2 + CO_2 \quad \Delta H = -41 \text{ kJ·mol}^{-1} \quad (9)$$

Factorial design center points and step sizes were based on parametric test results. Analysis of main effects, second order effects, and higher order effects, identified a path of steepest descent (POSD) toward optimal operating conditions. After the system stabilized, a minimum of four samples were taken at ten minute intervals for each set of operating conditions. Multiple samples provided data to calculate a mean, standard deviation, and confidence intervals at each test point.

Table 2
Base case variable values for parametric tests.

Variable	Base case value	Range of values for parametric test
Electrode gap distance	25 mm	Fixed
Axial exit size	12.5 mm	Fixed
Volumetric flow rate	3.5 slpm	Fixed
Oxygen input	0.43 slpm	Fixed
Nitrogen input	1.54 slpm	0.85 slpm–2 slpm
biogas input	1.54 slpm	0.4 slpm–2.48 slpm
Power input	220 W	140 W–300 W
Steam input	0.31 g min^{-1}	0.08–1.84 g min^{-1}
Sulfur input	0 ppm	0–45 ppm

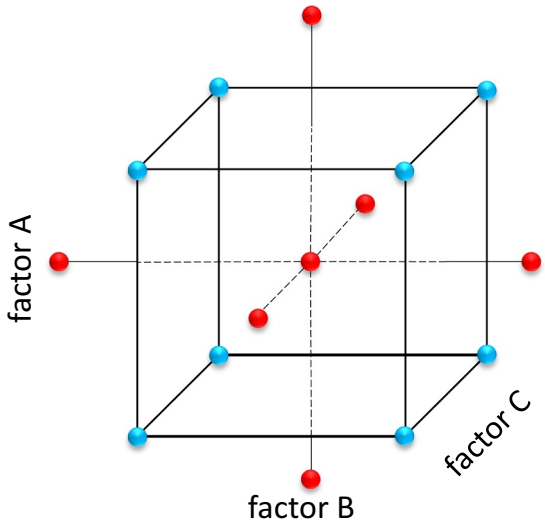

Fig. 4. Three factor central composite design schematic showing the axial points in red, and the cube points in blue. (For interpretation of the references to color in this figure legend, the reader is referred to the web version of this article.)

2.6.3. Central composite test design

Central composite design (CCD) augments the factorial design with a set of axial points as shown in Fig. 4. In order to find optimal conditions where factorial analysis has shown significant curvature between corner points and the center point, a CCD response surface design modeled the curvature and found the SER minima. The data was analyzed via Minitab® software package (Minitab Inc., State College, PA).

2.7. Data reduction

The following equations define standardized performance indicators for plasma reformers proposed by Petipas et al. and derived from the primary experimental test data [19].

Eq. (10) defines hydrogen yield as the ratio of hydrogen atoms as molecular hydrogen in the reformate gas to the hydrogen atoms in the input fuel.

$$\text{Hydrogen Yield} = \frac{\text{Hydrogen Atoms in } H_2 \text{ in reformate}}{\text{Hydrogen Atoms in Feed Fuel}} \times 100(\%) \quad (10)$$

Eq. (11) defines hydrogen selectivity as the ratio of hydrogen atoms present in the reformate as diatomic hydrogen (H_2) to the total number of H atoms present in the dry reformate. Again, it is assumed that all CO present in reformate can be converted to hydrogen by the water gas shift reaction (Eq. (9)).

$$\text{Hydrogen Selectivity} = \frac{\text{Moles } H_2 \text{ Produced}}{2(\text{Moles } CH_4 \text{ Converted})} \times 100(\%) \quad (11)$$

Efficiency is defined as the ratio of chemical enthalpy of the H_2 present in the reformate to the total power input to the reactor - including the input plasma power and the enthalpy of the injected fuel flow. As seen in Eq. (12), $\dot{m}$ and *LHV,* are mass flow rate and lower heating values of identified species, respectively.

$$\text{Efficiency } \eta = \frac{\text{LHV}_{H_2 \text{ gas}} \bullet (\dot{m}_{H_2} + \dot{m}_{CO})_{\text{produced}}}{\text{Plasma Power} + (\text{LHV}_{\text{fuel}} \bullet \dot{m}_{\text{fuel input}})} \times 100(\%) \quad (12)$$

Eq. (13) defines methane conversion as the reactor's ability to

convert methane into other species.

$$\text{Methane conversion} = \frac{(\dot{m}_{CH_4})_{\text{in fuel}} - (\dot{m}_{CH_4})_{\text{in reformate}}}{(\dot{m}_{CH_4})_{\text{in fuel}}} \times 100(\%) \quad (13)$$

Depending on the focus of the reforming application, performance parameters such as O_2 or H_2O conversion or CO selectivity or yield may also of importance and could be calculated with simple modification to these equations.

3. Results and discussion

In this section the results of parametric tests, factorial tests, and response surface tests (central composite design) are summarized and discussed.

3.1. Parametric tests

This section discusses the parametric test results from the investigation of the effects of four independent variables, EQR, SCR, power input, and H_2S input. Response of system performance metrics as a function of equivalence ratio are shown in Fig. 5. Methane conversion decreases approximately 40% as EQR decreases from a high of 0.7 to 0.1. To reduce EQR, the air flow rate to the reactor is held constant while increasing the fuel flow rate, producing a more fuel-rich input mixture. Efficiency and H_2 yield increase 10 to 15% (absolute) as the EQR decreases. Over the same range selectivity increases roughly 30% (absolute). The decreasing EQR also resulted in an exponentially decreasing SER values from 1017 kJ/mol of H_2, toward an asymptotic value of 285 kJ/mol of H_2 produced. Thus, the higher the biogas input to the system the better the reformer performed as measured by the decreasing SER value. All indicators of system performance are comparable with similar system operated on pure methane [4].

The effect of steam to carbon ratio was investigated while keeping EQR, power and inlet dry gas flowrate constant at 0.14, 220 W, and 3.5 lpm, respectively, while varying the steam input. Fig. 6 indicates that across a SCR range from 0 (POX conditions) to 3.0, the H_2 yield increases from 22% to 27.5%, while efficiency decreases ~4% from 26.8% to 22.7%. CH_4 conversion also showed an 8% reduction from 64% to 56%. Increasing SCR resulted in an increase in SER from 290 to 345 kJ/mol H_2. H_2 selectivity increased linearly across the SCR range, from 34 to 49% indicating that the decrease in methane conversion did not result in decreased H_2 productivity. With the exception of hydrogen yield and selectivity, system performance parameters show similar trends to those measured for pure methane reforming [4]. The

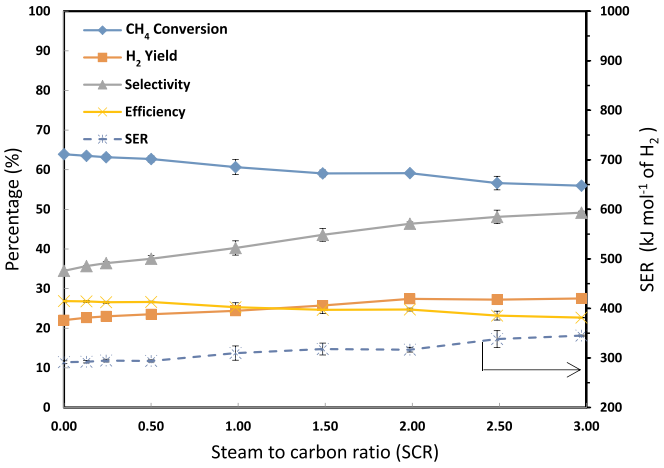

Fig. 6. Steam to carbon ratio parametric test results for biogas without H_2S. Error bars indicate 95% confidence interval. Error bars that are not visible are equal to or smaller in size than the data point symbol.

increasing SCR for biogas tests increased hydrogen yield and selectivity whereas similar tests on methane [4] found that selectivity remained constant and hydrogen yield decreased from 30.9% at an SCR of 0.5, to 17.0% at an SCR of 3.0. The difference may be the result of high CO_2 concentrations present in the biogas inhibiting reactions. The slight increase in SER (by 55 kJ/mol H_2 from zero steam to SCR = 3.0) with increasing SCR can be explained by the higher energy needed to energize water molecules.

The parametric test for power input to the plasma began at 280 W and incrementally decreased the power input until the arc could no longer be sustained. Fig. 7 indicates increasing power results in linear increases in all indicators of system performance, albeit at different rates. The slope of the SER response was the steepest, increasing from 255 kJ/mol of H_2 at 140 W to 345 kJ/mol of H_2 at 280 W, a 35% (relative) increase. Methane conversion, the second most sensitive parameter, increased 25% (relative) over the test range, while H_2 yield increased by ~32% (relative). Selectivity and efficiency remained fairly constant with increases on the order of 2% (absolute).

Fig. 8 shows the parametric test results of varying H_2S content in the bio-gas input flow. H_2S contents of 5.3 to 45.4 ppm in the biogas flow resulted in 2.3 to 19.9 ppm H_2S in the bulk inlet gas stream. Over this range, H_2S reformate concentrations increased from 0.047 to 0.171 ppm, while SO_2 increased linearly from 0.47 to 0.82 ppm. This

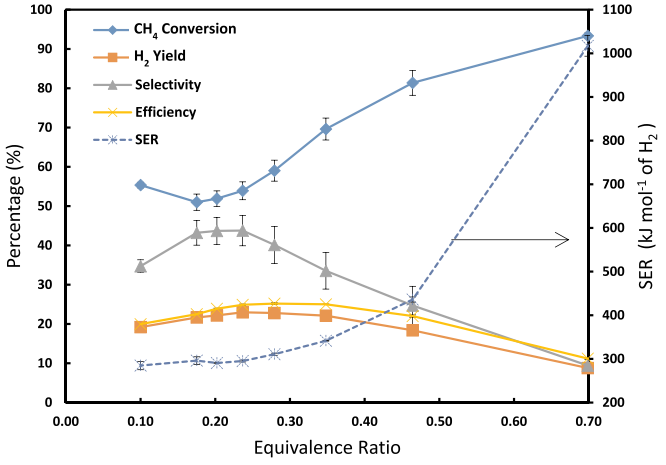

Fig. 5. EQR parametric test results for biogas with no H_2S input. Error bars indicate 95% confidence interval. Error bars that are not visible are equal to or smaller in size than the data point symbol.

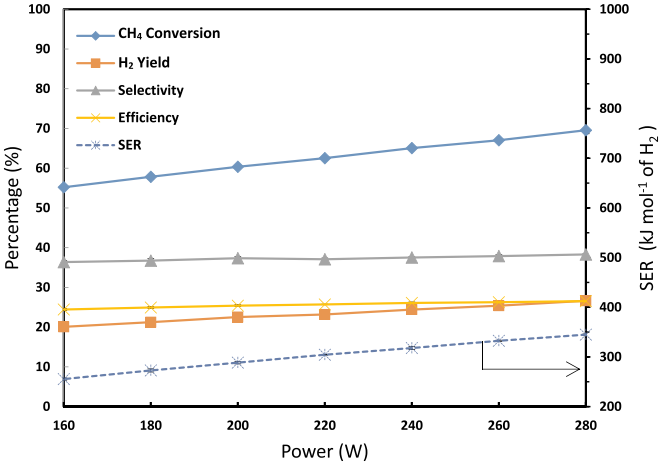

Fig. 7. Power input parametric test for biogas without H_2S. Error bars indicate 95% confidence interval. Error bars that are not visible are equal to or smaller in size than the data point symbol.

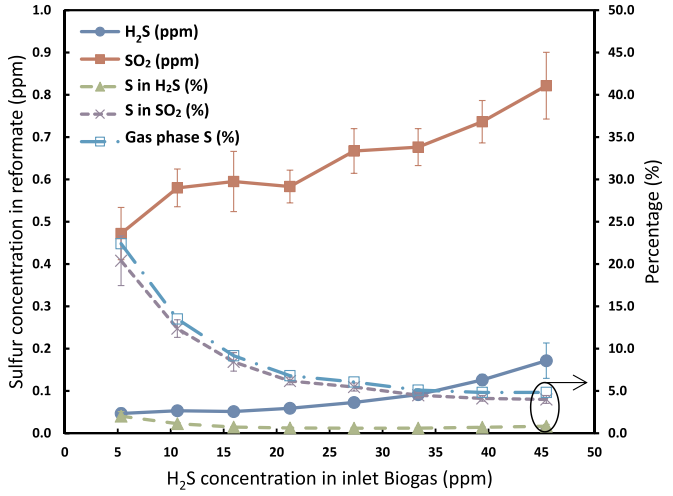

Fig. 8. H_2S input parametric test. Error bars indicate 95% confidence. Error bars that are not visible are equal to or smaller in size than the data point symbol.

indicates the great capability of the proposed system by removing 88% of the sulfur species at the 5.3 ppm input test condition to 94.8% removal at 45.4 ppm input. The right axis at Fig. 8 shows how the ratio of sulfur detected in the reformate gas to the sulfur in the inlet changes with increasing H_2S inlet concentration. The remaining sulfur compounds in the gas stream exponentially decreased approaching an asymptote of ~5%. However, these measurements must be viewed qualitatively as all H_2S concentrations were below the GC-SCD's calculated lower detectable limit (LDL) of 0.21 ppm, and the majority of the SO_2 was detectable but under the 0.70 ppm calculated lower quantitative limit (LQL).

3.2. Factorial tests

The following sections present test results for the factorial tests and response surface methodology (RSM) approach to finding optimum operating conditions for biogas as a feedstock for the NTP reformer.

The center point for the factorial tests was selected based on parametric test results and is summarized in Table 3. The −1 and +1 designations in Table 3 show the center point minus and plus the step size respectively.

Table 4 summarizes the main effects of the three input variables EQR, SCR, and power, along with second and third order interaction effects. Assuming the highest order effects are negligible [52], the third order effect can be considered as an estimate of error for the system. Hence, only effects with absolute values > 105% of the absolute value of the third order effect (ABC) were considered significant.

First order effects indicate that increasing the EQR has significant negative effects on all performance parameters except methane conversion. Increasing the EQR has positive effects on methane conversion as conditions approach stoichiometric AFR and complete oxidation. Increasing the SCR has a slight positive effect on methane conversion but does not produce significant effects in any of the other performance

Table 3
First full factorial center point and step sizes for NTP testing of biogas without H_2S.

	−1	Center Point	+1	Step size
EQR	0.32	0.4	0.48	0.08
SCR	0.75	1.0	1.25	0.25
Power (W)	200	220	240	20

Table 4
Effect summary for the first factorial test on biogas without H_2S. Values represent the change in the performance value resulting from increasing the independent variables from the −1 to the +1 values shown in Table 3.

	Responses	Methane conversion, change (%)	Hydrogen yield, change (%)	Hydrogen selectivity, change (%)	Efficiency, change (%)	SER, change (kJ/mol H_2)
1st order effects	A (EQ ratio)	11.9[a]	−4.5[a]	−10.5[a]	−3.5[a]	103.0[a]
	B (SC ratio)	4.5[a]	−0.4	−2.3	−1.7	23.3
	C (Power)	7.2[a]	1.3[a]	−0.9	−0.1	42.0[a]
2nd order effects	AB	4.6[a]	−0.3	−2.3	−0.7	11.1
	AC	6.9[a]	−1.0	−3.9[a]	0.2	2.0
	BC	−6.3[a]	0.0	2.6	−1.2	9.0
3rd order effects	ABC	−3.8	1.0	2.7	2.9	−32.9

[a] Indicates significant effect, |effect| > |(1.05*ABC)|.

Table 5
Redesigned second full factorial center point and step sizes.

	−1	Center point	+1	Step size
EQ ratio	0.12	0.16	0.2	0.04
SC ratio	0.2	0.3	0.4	0.1
Power(W)	150	160	170	10

indicators. Increasing power improves methane conversion and hydrogen yield but negatively impacts SER performance and has no effects on other performance indicators.

Second order effects indicate that increasing EQR and SCR in tandem produces an additional 5% methane conversion. Increasing EQR and power in tandem resulted in an additional ~7% increase in methane conversion but with an additional 4% reduction in H_2 selectivity. Increasing power and SCR at the same time provided an additional ~6% decrease in methane conversion.

Although the factorial results showed SCR effects to be insignificant, decreasing steam input lowers steam generation energy costs and was included in the path of steepest descent (POSD) analysis. Before running the POSD tests, low-steam reactor stability was tested and verified. The POSD was characterized by decreasing all three variables until reaching system limits (arc extinction).

Based on the POSD results, center point and step sizes for the second factorial test are summarized in Table 5. This factorial test analyzes the response surface around the new center point to see if there is a further possible reduction in the SER.

Table 6 summarizes the results for the second factorial test. The results indicate the effects of all three factors are significant, and suggest decreasing all three factors for the next path of steepest descent. ANOVA analysis however, shows a curvature *P*-value of 0.01 (< 0.05) indicating significant curvature [52] between corner points and the center point. This suggests that the reactor is at near optimal conditions. Therefore, a central composite test was designed as explained in Section 2.6.3 and was performed to model the response curvature.

3.3. Response surface analysis

A central composite design (CCD) added six axial points to the last factorial test, and resulted in a quadratic surface model for SER response. The global minima on this surface identified operating conditions producing a minimum SER value.

The optimum operating point required 160 W of plasma power, due to occasional arc instability at 150 W. Optimal conditions were defined by an EQR of 0.11, an SCR of 0.14, and 160 W of arc power and a 3.5 slpm dry gas input composed of 0.25 slpm O_2, 0.95 slpm N_2, 2.30 slpm of biogas, and 0.13 g min^{-1} steam input. These conditions produced a reformate flowrate of 3.71 slpm and the associated gas composition translated to a CH_4 conversion of 49%, a H_2 yield of 23%, a H_2 selectivity of 48%, an efficiency of 25%, and SER of 184.18 kJ/mol H_2 (1.91 eV/H_2 molecule). The latter is significantly below the 3.37 eV/H_2 molecule produced for conventional steam reforming of methane [53]. The optimal conditions reported apply to this specific non-thermal plasma reactor and their applicability at larger scales [54–56] should be investigated. Note that opportunities for system integration could be expected to improve overall system performance.

3.4. Comparison with thermochemical simulation

FactSage™ (CRCT, Montreal, Quebec, Canada) software package was used to calculate the equilibrium gas composition for the optimal input conditions. The arc power was used as the input value for the change in enthalpy between reactants and products, the experimental reactant flow rates were used as relative molar ratios of input reactants, and the equilibrium calculation was performed at 298 K, 1 bar. Table 7

Table 6
Effect summary for the second factorial test on biogas without H_2S.

Responses	Methane conversion, change (%)	Hydrogen yield, change (%)	Hydrogen selectivity, change (%)	Efficiency, change (%)	SER, change (kJ/mol H_2)
A (EQ ratio)	13.9[a]	2.3[a]	−7.9[a]	3.3[a]	11.7[a]
B (SC ratio)	−1.5[a]	0.4[a]	1.9[a]	−0.6[a]	4.6[a]
C (Power)	3.0[a]	1.2[a]	−0.4	1.1[a]	12.2[a]
AB	−0.5[a]	0.3	0.6	−0.2	−0.2
AC	0.1	−0.1	−0.1	−0.1	−0.2
BC	−0.1	0.1	0.3	−0.1	−0.3[a]
ABC	0.4	−0.2	−0.8	0.2	−0.2

[a] Indicated significant effect, $|\text{effect}| > |(1.05*\text{ABC})|$.

Table 7
Experimental results at the non-thermal plasma optimum operating point and results from thermochemical equilibrium calculation using optimum point input conditions.

	H_2 (%)	N_2 (%)	CO (%)	CH_4 (%)	CO_2 (%)	Other (%)
Thermochemical equilibrium	35.19	18.94	31.50	3.77	10.60	0.00
Experimental	14.24	31.87	16.99	15.68	20.38	0.84

compares reformate gas composition from the thermochemical equilibrium calculation with the experimental gas composition from the optimal point. Table 7 data were used to calculate ideal performance metrics for both equilibrium and experimental conditions, summarized in Table 8. Thermochemical equilibrium calculations yielded an efficiency of 71% with 82% of reformate hydrogen predicted to be present as H_2 and 18% as CH_4. Differences between the experimental optimal point and calculated values are attributed to the non-ideality of the system. From a thermodynamic stand point, heat loss, incomplete mixing of reactants, and inadequate retention time of reactants in the reaction chamber, all contribute to non-ideal conditions.

3.5. Sulfur fate

This section discusses the fate of sulfur compounds in the biogas input stream. Detection limits prevented factorial optimization of H_2S removal, however, 180 min duration center-point tests conducted at three unique operating conditions provided solid, liquid, and gas samples which further utilized in analyzing the fate of sulfur in the system. The operating conditions, summarized in Table 9, resulted in an average SER of 312.79 kJ/mol H_2 (3.26 eV/H_2 molecule produced) for the three points). During these 180 min tests, 8.96 mg of sulfur was input to the system. Ultimately 46.5 ± 26.7% of the input sulfur was accounted for in the solid, liquid and gas analyses.

To confirm that the plasma arc contributed to the removal of H_2S, 20 ppm H_2S in biogas with accompanying air and steam mixtures was injected into the reformer and allowed to pass through the system without the plasma arc energized. The outlet gas was analyzed and the concentration of H_2S was identical to the inlet indicating that the design modification to make the working surfaces of the system inert to sulfur was successful. Additionally, the H_2S biogas mixture was passed through the reactor without the arc energized and then through the impingers containing both IPA and deionized H_2O. The H_2S concentration in the outlet stream was unchanged from the inlet.

Similar tests explored the fate of SO_2 at 25 ppm in the bulk inlet gas passing through the system. When injected into the reactor without the presence of steam, SO_2 suffered minimal losses. However, when steam was injected into the reactor as well, without the arc engaged, H_2SO_4 formed. This caused the SO_2 concentration in the outlet gas stream to drop from 24.8 ppm to 0.72 ± 0.09 ppm, and the liquid recovered from the first impinger ultimately contained 59.9 ppm of sulfate. These results confirm the performance of the proposed system in cleaning the H_2S contaminant from the inlet biogas. Even in case the NPT reactor converts H_2S to SO_2, results indicate it can be removed with minimal effort with water scrubbing.

21.25 ppm H_2S in biogas was metered into the system, resulting in 9.35 ppm concentration in the bulk reactant stream. The plasma reforming removed the majority of H_2S, leaving 0.069 ± 0.026 ppm on average in the reformate – less than the LDL of 0.21 ppm. Due to the oxidation of H_2S into SO_2 via the reaction in Eq. (4), SO_2 was found in detectable, but not quantifiable amounts. Ultimately 5.7 ± 0.4% of the initial sulfur appeared to remain in the gas stream.

Oxidation of a portion of the H_2S stream resulted in the production of SO_2. The SO_2 in turn reacted with steam present in the reformer to form H_2SO_4, sulfuric acid. The first impinger in the impinger train, initially filled with 100 ml of IPA, captured both condensed steam and sulfuric acid. After 180 min of operation the impingers on average contained 249.6 ± 29.5 ml of solution.

Impinger solution had a pH value of 3.8 as measured by the AR25 Dual Channel pH/Ion meter. The Dionex ICS-1100 Ion Chromatograph detected on average 17.6 ± 14.0 ppm sulfate ions. This corresponded to 3.4 ± 2.2 mg of sulfur, or 38.2 ± 24.8% of the input sulfur.

Images A and B in Fig. 9 show the solid particles in situ on the PTFE liner, while image C shows the solid particles scraped from the liner onto the targeting stub. The solid formations, rods, plates, and spheres, in images A and B were crushed when scraped onto the targeting stub.

Unfortunately, the solids would decay and 'wander' when exposed to the electron beam. This impeded the image quality and the identification of species present in the solids. On average, solid composition as determined by EDS was primarily oxygen (81.3 ± 3.3%), carbon (15.6 ± 3.0%), and sulfur (2.8 ± 0.8%). Some particles subjected to EDS contained 19.5% sulfur by mass, however, the large majority of particles contained ≤5%. Recoverable amounts of solid sample limited the analytical effort, however future work should explore transmission electron microscopy and thermogravimetric analysis as tools for identifying solid composition.

Of the three phases, the recovered solid contained 2.6 ± 1.5% of the input sulfur, the smallest of the three fractions. Sulfur in gaseous form accounted for about 5% of the input sulfur. Finally, sulfur recovered in liquid form accounts for 38.2 ± 24.8% of the input sulfur. This indicates that the proposed system removes hydrogen sulfide impurities from biogas while performing reformation into hydrogen rich gas. Further steps include study on higher flow rates and higher concentration of impurities. However, the current study range showed improvement in performance of the proposed system in removing hydrogen sulfide impurities as concentration increased.

3.6. Comparison to other works

There is interest in upgrading biogas to biomethane as a substitute for natural gas and removing H_2S is a typical unit operation. Research has also focused on reforming H_2S to produce hydrogen (see eq. 6), or to simply remove it. Process results for synthetic biogas containing H_2S reformed to a hydrogen rich stream in a non-thermal plasma reactor

Table 8
Performance parameters for experimental and thermochemical calculation results of Table 7.

	CH_4 conversion (%)	H_2 yield (%)	H_2 selectivity (%)	Efficiency (%)	SER (kJ/mol H_2)
Thermochemical equilibrium	92	81	89	71	64
Experimental	49	23	48	25	184

Table 9
Operating point input conditions for sulfur fate study.

	EQ ratio	SCR	Power (Watts)	SER (kJ/mol H_2)
First operating point	0.24	1	240	286.71
Second operating point	0.3	1.75	260	333.42
Third operating point	0.3	1	260	318.24

reported here are, unfortunately, nearly impossible to compare to the literature due to lack of comparable studies. Comparisons are made in three relevant areas; studies using non-thermal plasma in order to reform biogas at atmospheric pressure (see Table 10), methods of treatment of biogas in order to remove H_2S (see Table 11), and methods of reforming H_2S by different plasma technologies (see Table 12).

Table 10 indicates that gliding arc methods have the lowest energy costs. The summarized research includes inlet gas composition that contain only CH_4 and CO_2 [57–59], biogas with O_2 added [47,60], biogas with air [49,57,61], and finally biogas with air and steam [30,49]. The inlet flowrates range from 0.1 slpm to 24 slpm. A direct comparison is often impossible due to different system specifications, but the standardized performance indicators proposed by Petipas et al. [19] for plasma reformers have been applied, to the extent possible, within the limits of the available data. The closest results resembling the gas composition for the current work are those that included steam in the inlet gas. Pornmai et al. [30] work on simulated natural gas with hydrocarbon to O_2 ratio of 2:1 and 0.13 SCR resulted in a SER value of 7.62 eV/H_2 molecule produced. To confirm that steam does not directly produce hydrogen in the plasma reactor, Pornmai et al. [30] flowed a 2:1, He:O_2 mixture with 10% (mole) steam flow under the same plasma operating conditions and observed no H_2 in the outlet stream. Chun et al. [31] attained an SER of 3.0 eV/H_2 molecule produced with a gliding arc reformer and secondary catalyst bed operating on an inlet gas composition of 60% CH_4 and 40% CO_2 and an SCR of 3 (no oxygen was reportedly used). Liu et al. [62] achieved an SER of 1.6 eV/H_2 molecule produced with a high CO_2 concentration in the inlet gas; CH_4:CO_2 of 2:3. Liu et al. [49] also reformed simulated biogas with air addition, without steam, and at high inlet flow rate of 15 slpm, reducing the SER to 0.70 eV/H_2 molecule produced. The latter work differs from the conditions reported here by having a higher CH_4 concentration in the inlet gas, by excluding added steam, and by operating at a higher input flow rate (15 slpm compared to 3.66 slpm).

The information in Table 11 indicates that the H_2S removal methods have high removal efficiency but just until the absorbent saturation and H_2S breakthrough. Except for Jones et al. which had ~96% removal efficiency in two days of run, none of the methods are comparable to the plasma reforming method in terms of long term of operable time without stopping the system. The non-thermal plasma reactor in the present study showed > 95% H_2S removal efficiency reaching below 0.4 ppm; from the synthetic LFG (50–50% CH_4-CO_2) contaminated with

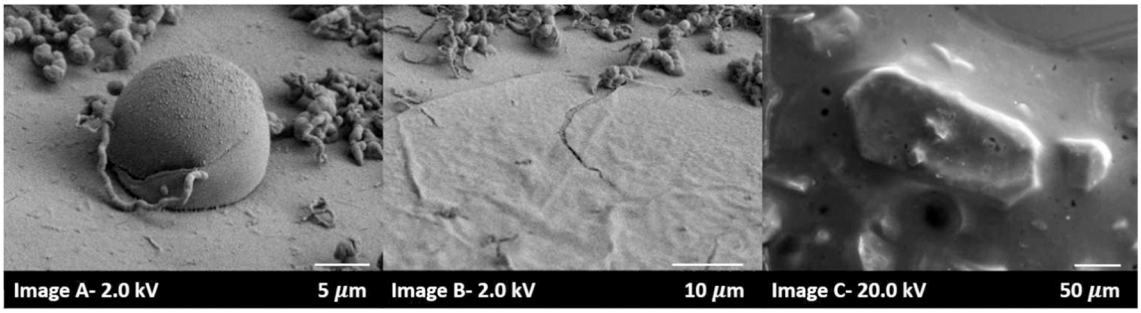

Fig. 9. SEM imaging of solid particles recovered from the PTFE impinger liner. Image A - Solids and rods. Image B - Plates and rods. Image C - recovered solid particles in place on SEM target.

Table 10
Non-thermal plasma assisted reforming of biogas comparison table - at atmospheric pressure.

Plasma reactor type [Reference]	Inlet gas composition (molar ratios)	CH_4/CO_2	Inlet total flow rate (slpm)	CH_4 conversion (%)	H_2 selectivity (%)	SER (eV/H_2 molecule) (kJ/mol H_2)	Efficiency (%)
Corona discharge [58]	CH_4:CO_2, 1:1	1/1	0.6	27.8	55.1%	7.02 (675. 6)	na[a]
Gliding arc discharge (spiral electrode) [49]	CH_4:CO_2:O_2:N_2, 3:2:1.8:6.8	3/2	15	77	~57	0.70 (66)	na[a]
Gliding Arc discharge (flat electrode) [61]	CH_4:C_2H_6:C_3H_8:CO_2:O_2:N_2, 14:1:1:4:10:37.6	7/2	0.125	~32	~48	16.60 (1600)	na[a]
Spark discharge [60]	CH_4:CO_2:O_2, 6:4:7	3/2	N/A	77	77	3.5 (340)	na[a]
Gliding arc tornado discharge [62]	CH_4:CO_2, 2:3	2/3	10	29	~79	1.6 (153.8)	68
Laval nozzle arc discharge [59]	CH_4:CO_2, 41.7:58.3	~41/58	24	47	13	285 W	na[a]
Microwave discharge [47]	CH_4:CO_2:O_2, 2.3:1:1	2/3	1	67.12	12.84	800 W	na[a]
Gliding Arc Discharge (SR and POX) [30]	CH_4:C_2H_6:C_3H_8:CO_2:O_2, 70:5:5:20:50	7/2	0.1	19	68.2	7.62 (732.7)	na[a]
Gliding arc discharge and catalyst reformer [31]	CH_4:CO_2, 6:4	3/2	16	100	59	3.00 (289)	53
Gliding arc discharge (co-axial electrode, thermally insulated reactor, with catalyst) [32]	CH_4:CO_2:O_2, 3:2:1.8	3/2	4	~50	~35	0.5 (48)	50, 86[b]
GAT reverse vortex flow [present work]	CH_4:CO_2:O_2:N_2:H_2O, 1:1:0.2:0.8:0.14	1/1	3.66	48.8	47.8	1.91 (183.6)	25.3

[a] na = energy efficiency data per Eq. (12) above was not reported in this reference.

Table 11
Features of H_2S removal methods.

Method	Inlet stream	H_2S concentration in carrier gas	Moisture content	Removal efficiency	Flow rate	Temperature	Notes	Ref.
Activated Carbon (AC)	CO_2-N_2 (50%-%50%)	50 ppm	N/A	100% adsorption before breakthrough at 5 ppm. (~300 min)	0.200 L·min^{-1}	303 K	Capacity loss of about 15% in each adsorption/ regeneration cycle. Regeneration does not recommended	[15]
Silica gel	Biogas (from digester)	1600 ppm	Dewatered	100% for 90 min, then dropped quickly	1.9 L·min^{-1}	Room temperature	Dewatered or else H_2S competes for binding sites	[63]
Coal bottom ash	Pre-humidified Air	100–300 ppm	N/A	100% for 15 min. > 70% 120 min	1.1–4.4 L·min^{-1}	Room temperature	100% for 100 ppm in 1.1 L/min during all 8 Hours of the test	[64]
Molecular sieve	Mixture of H_2S/CH_4	5%	N/A	42.3 mg-H_2S/g-material for 22.3 min until reaches 100 ppm	0.005 L·min·	Room temperature	The best reported sieve materials were impregnated with 10 wt% of Zn and 20 wt% of Cu	[65]
Iron sponge	Biogas (from food waste digester)	700–1000 ppm	15% moister in sponge	89% and 91%	1.0 L·min^{-1}	Room temperature		[66]
Activated carbons	LFG in Genoa	Mean concentration 245 pmm	N/A	10.88% kgH_2S_{ads}/kgAC	500 Nm^3·hr^{-1} (8333 L·min^{-1})	Room temperature	The GSHV was about 335 h^{-1} during the tests. Outlet H_2S concentration of 1 ppm was observed	[67]
Biofilter	Humidified air	50 ppmv	60%	95%–96%	8.14 g·H_2S·m^3·hr^{-1}	303 K	2 days of operation	[68]

Table 12
Plasma assisted H_2S removal method comparison.

Method	Inlet stream	H_2S concentration	Pressure	H_2S conversion %	Specific energy requirement (eV/H_2 molecule)[a,b]	Reference
Pulsed corona discharge	Argon	16% molar	134 kPa	10	17.4	[36]
Pulsed corona discharge	Ar-N_2 (50–50% molar)	8% molar	134 kPa	44	4.9	[69]
Dielectric barrier discharge	Ar-N_2	20–100%	Atmospheric pressures	0.5–12%	50	[40]
Dielectric barrier discharge	Argon	25 vol%	Atmospheric pressures	~16%	1.6	[70]
Rotating glow discharge	Hydrogen	30%	Atmospheric pressures	~10%	27	[71]
Gliding Arc plasma	Diluted in Air	50 ppm	Atmospheric pressures	75%	~500	[44,45]
Gliding arc in tornado	14 slpm H_2S	100%	Atmospheric pressures	25%	1.2	[37]
Gliding arc in tornado	14 slpm H_2S + 2.8 slpm O_2	83%	Atmospheric pressures	50%	1.0	[46]
This work (GAT[c] reverse vortex flow)	Synthetic biogas	21 ppm	Atmospheric pressures	> 94%	3.26	This work

[a] 1 kJ/mol.H_2 = 0.0104 eV/H_2 molecule.
[b] Specific energy ratio for all literature studies are based on H_2 produced from H_2S whereas the present work also includes H_2 produced from CH_4.
[c] GAT = gliding arc tornado.

21 ppm H_2S (10 ppm in total input dry gas to the reactor). Moreover, most of the methods require regeneration of the adsorbent. In most cases, the references do not recommend regeneration due to the decay of efficiency. As discussed in the introduction the non-thermal plasma reactor does not require change of parts, e.g. electrodes, as other plasma methods may require due to corrosion.

Table 12 compares specific energy requirement for H_2S conversion in different types of plasma reactors. None of the methods is comparable to > 95% H_2S conversion as demonstrated in the current results. The next highest conversion in the table, 75%, was achieved with a gliding arc plasma reactor operating on 50 ppm H_2S diluted in air at a relatively high SER value, 500 eV/H_2 molecule [45] [48]. The considerably lower value of 3.26 eV/H_2 molecule produced in the current work reflects that the bulk of the H_2 was produced from CH_4 rather than from the conversion of H_2S. The second highest conversion value, 50%, was also from a gliding arc method. Nunnally et al. first tested adding tornado effect to the gas stream of a gliding arc plasma reactor and could reach an SER value of 1.2 eV/H_2 molecule produced in converting 25% of their 14 slpm flow of pure H_2S [37] [49]. They modified their method by adding 2.8 slpm O_2 (equal to 20% of the pure H_2S flow) and reached 50% conversion with SER value of 1.0 eV/H_2 molecule [46] [50]. The present work demonstrated > 95% conversion of 21 ppm H_2S in biogas with a SER value of 3.26 eV/H_2molecule produced. Parametric test varying H_2S concentration in the present work showed increasing H_2S conversion with increasing H_2S concentration up to the maximum value tested, ~50 ppm in biogas.

4. Conclusions

An experimental investigation was conducted to reform biogas into a hydrogen-rich gas stream and to characterize the fate of H_2S present as a contaminant for the first time. For this purpose, a non-thermal plasma reactor was modified and systematic experiments designed and performed. Parametric, factorial, and response surface methodology (RSM) tests conducted sequentially identified the best reactor operating conditions that minimized specific energy requirements (kJ/mol H_2).

Optimal operating conditions of EQR = 0.11, SCR = 0.14, and 160 W of arc input power resulted in a minimized SER of 184 kJ/mol H_2 for the reactor running on simulated landfill biogas (50% methane, 50% carbon dioxide). At these conditions, the reformate gas composition was 14.2% H_2, 31.9% N_2, 17.0% CO, 3.8% CH_4, and 10.6% CO_2, resulting in methane conversion of 48.8%, a hydrogen yield of 23.4%, hydrogen selectivity = 47.8%, and an efficiency of 25.3%. The obtained 185 KJ/mol H_2 is well below ~340 kJ/mol H_2 for steam reforming of natural gas. This performance was also well below other plasma conversion methods and indicates the suitability of gliding arc reverse vortex flow plasma in biogas conversion.

Results from H_2S conversion tests determined that approximately 5.7% of the sulfur input to the system as 21 ppm H_2S in biogas was recovered as H_2S in the dry outlet reformate stream, resulting in ~94% H_2S conversion. The remainder of the sulfur was converted to SO_2 that was captured as H_2SO_4 in downstream impingers or recovered as a solid of unknown molecular structure on PTFE tubing surfaces between the reformer and the impingers. This great conversion efficiency indicates the capability of the proposed system for simultaneous removal of hydrogen sulfide contaminants from inlet biogas beside reforming hydrocarbons into hydrogen rich gas.

Future research should identify optimal conditions for biogas reforming at higher input flowrates as an approach to a more industrialized scale and optimize operating conditions for sulfur removal and for a wider range of contaminant sulfur species.

Acknowledgements

This work was supported by the Center for BioEnergy Research and Development, a National Science Foundation, Industry/University Cooperative Research Center [Award No. IIP-0832554] and the Office of Naval Research (Grant Number N00014-12-1-0496).

References

[1] F. Mueller-Langer, E. Tzimas, M. Kaltschmitt, S. Peteves, Techno-economic assessment of hydrogen production processes for the hydrogen economy for the short and medium term, Int. J. Hydrog. Energy 32 (16) (2007) 3797–3810.
[2] R. Kothari, D. Buddhi, R. Sawhney, Comparison of environmental and economic aspects of various hydrogen production methods, Renew. Sust. Energ. Rev. 12 (2) (2008) 553–563.
[3] S. Samsatli, N.J. Samsatli, The role of renewable hydrogen and inter-seasonal storage in decarbonising heat–Comprehensive optimisation of future renewable energy value chains, Appl. Energy 233 (2019) 854–893.
[4] W. Piavis, S. Turn, An experimental investigation of reverse vortex flow plasma reforming of methane, Int. J. Hydrog. Energy 37 (22) (2012) 17078–17092.
[5] E. El Ahmar, C. Met, O. Aubry, A. Khacef, J. Cormier, Hydrogen enrichment of a methane–air mixture by atmospheric pressure plasma for vehicle applications, Chem. Eng. J. 116 (1) (2006) 13–18.
[6] L. Bromberg, D. Cohn, A. Rabinovich, N. Alexeev, Hydrogen manufacturing using low current, non-thermal plasma boosted fuel converters, (2001).
[7] Methane conversion into syn-gas in gliding arc discharge, in: K. Iskenderova, P. Porshnev, A. Gutsol, A. Saveliev, A. Fridman, L. Kennedy, et al. (Eds.), 15th International symposium on plasma chemistry, 2001 Orleans.
[8] C.S. Kalra, A.F. Gutsol, A.A. Fridman, Gliding arc discharges as a source of intermediate plasma for methane partial oxidation, IEEE transactions on plasma science. 33 (1) (2005) 32–41.
[9] Methane Steam reforming with oxygen in a sliding discharge reactor, in: F. Ouni, A. Khacef, J. Cormier (Eds.), 17th International Symposium on Plasma Chemistry proceedings, ISPC, 2005.
[10] G. Tchobanoglous, H. Theisen, S.A. Vigil, V.M. Alaniz, Integrated solid waste management: engineering principles and management issues, McGraw-Hill New York, 1993.
[11] EPA U, Global mitigation of non-CO2 greenhouse gases: 2010-2030, United States Environmental Protection Agency Washington (DC), 2013.
[12] P.K. Cheekatamarla, A.M. Lane, Catalytic autothermal reforming of diesel fuel for hydrogen generation in fuel cells: I. Activity tests and sulfur poisoning, J. Power Sources 152 (2005) 256–263.
[13] R. Mohtadi, W.-K. Lee, S. Cowan, J. Van Zee, M. Murthy, Effects of hydrogen sulfide on the performance of a PEMFC, Electrochemical solid-state letters. 6 (12) (2003) A272–A274.
[14] L.F. Brown, A comparative study of fuels for on-board hydrogen production for fuel-cell-powered automobiles, Int. J. Hydrog. Energy 26 (4) (2001) 381–397.
[15] G. Monteleone, M. De Francesco, S. Galli, M. Marchetti, V. Naticchioni, Deep H2S removal from biogas for molten carbonate fuel cell (MCFC) systems, Chem. Eng. J. 173 (2) (2011) 407–414.
[16] P. Jamróz, W. Kordylewski, M. Wnukowski, Microwave plasma application in decomposition and steam reforming of model tar compounds, Fuel Process. Technol. 169 (2018) 1–14.
[17] Y. Li, Y. Wang, X. Zhang, Z. Mi, Thermodynamic analysis of autothermal steam and CO2 reforming of methane, Int. J. Hydrog. Energy 33 (10) (2008) 2507–2514.
[18] A. Czernichowski, GlidArc assisted preparation of the synthesis gas from natural and waste hydrocarbons gases, Oil Gas Sci. Technol. 56 (2) (2001) 181–198.
[19] G. Petitpas, J.-D. Rollier, A. Darmon, J. Gonzalez-Aguilar, R. Metkemeijer, L. Fulcheri, A comparative study of non-thermal plasma assisted reforming technologies, Int. J. Hydrog. Energy 32 (14) (2007) 2848–2867.
[20] L. Bromberg, D. Cohn, A. Rabinovich, N. Alexeev, A. Samokhin, K. Hadidi, et al., Onboard plasmatron hydrogen production for improved vehicles, (2006).
[21] W. Piavis, S. Turn, S.A. Mousavi, Non-thermal gliding-arc plasma reforming of dodecane and hydroprocessed renewable diesel, Int. J. Hydrog. Energy 40 (39) (2015) 13295–13305.
[22] M. Sobacchi, A. Saveliev, A. Fridman, L.A. Kennedy, S. Ahmed, T. Krause, Experimental assessment of a combined plasma/catalytic system for hydrogen production via partial oxidation of hydrocarbon fuels, Int. J. Hydrog. Energy 27 (6) (2002) 635–642.
[23] L. Liu, Q. Wang, S. Ahmad, X. Yang, M. Ji, Y. Sun, Steam reforming of toluene as model biomass tar to H2-rich syngas in a DBD plasma-catalytic system, J. Energy Inst. 91 (6) (2018) 927–939.
[24] T. Paulmier, L. Fulcheri, Use of non-thermal plasma for hydrocarbon reforming, Chem. Eng. J. 106 (1) (2005) 59–71.
[25] GlidArc-assisted reforming of carbonaceous feedstocks into synthesis gas. Detailed study on Propane, in: A. Czernichowski, M. Czernichowski, P. Czernichowski (Eds.), 16th International Symposium on Plasma Chemistry proceedings, ISPC, 2003.
[26] R.B. Biniwale, A. Mizuno, M. Ichikawa, Hydrogen production by reforming of iso-octane using spray-pulsed injection and effect of non-thermal plasma, Appl. Catal. A Gen. 276 (1-2) (2004) 169–177.
[27] Czernichowski A, Czernichowski P, Wesolowska K, editors. Plasma-catalytical partial oxidation of various carbonaceous feeds into synthesis gas. ASME 2004 2nd International Conference on Fuel Cell Science, Engineering and Technology; 2004: American Society of Mechanical Engineers.
[28] T. Wang, X. Zhang, J. Liu, H. Liu, Y. Guo, B. Sun, Plasma-assisted catalytic conversion of NO over Cu-Fe catalysts supported on ZSM-5 and carbon nanotubes at low temperature, Fuel Process. Technol. 178 (2018) 53–61.
[29] A.H. Khoja, M. Tahir, N.A.S. Amin, Cold plasma dielectric barrier discharge reactor

for dry reforming of methane over Ni/ϒ-Al 2 O 3-MgO nanocomposite, Fuel Process. Technol. 178 (2018) 166–179.
[30] K. Pornmai, A. Jindanin, H. Sekiguchi, S. Chavadej, Synthesis gas production from CO 2-containing natural gas by combined steam reforming and partial oxidation in an AC gliding arc discharge, Plasma Chem. Plasma Process. 32 (4) (2012) 723–742.
[31] Y.N. Chun, Y.C. Yang, K. Yoshikawa, Hydrogen generation from biogas reforming using a gliding arc plasma-catalyst reformer, Catal. Today 148 (3-4) (2009) 283–289.
[32] K. Li, J.-L. Liu, X.-S. Li, X. Zhu, A.-M. Zhu, Warm plasma catalytic reforming of biogas in a heat-insulated reactor: Dramatic energy efficiency and catalyst auto-reduction, Chem. Eng. J. 288 (2016) 671–679.
[33] F. Yang, S.M.A. Mousavi, T.K. Oh, T. Yang, Y. Lu, C. Farley, et al., Sodium–Sulfur Flow Battery for Low-Cost Electrical Storage, Adv. Energy Mater. 8 (11) (2018) 1701991.
[34] B. Meyer, Sulfur, energy, and environment: Elsevier, (2013).
[35] A. Fridman, S. Nester, L. Kennedy, Gliding arc gas discharge, Prog. Energy Combust. Sci. 25 (2) (1999) 211–231.
[36] G.-B. Zhao, S. John, J.-J. Zhang, J.C. Hamann, S.S. Muknahallipatna, S. Legowski, et al., Production of hydrogen and sulfur from hydrogen sulfide in a nonthermal-plasma pulsed corona discharge reactor, Chem. Eng. Sci. 62 (8) (2007) 2216–2227.
[37] T. Nunnally, K. Gutsol, A. Rabinovich, A. Fridman, A. Starikovsky, A. Gutsol, et al., Dissociation of H2S in non-equilibrium gliding arc “tornado” discharge, Int. J. Hydrog. Energy 34 (18) (2009) 7618–7625.
[38] E. Luinstra, Hydrogen from H2S: technologies and economics: Sulfotech Research, (1995).
[39] B.G. Cox, P.F. Clarke, B.B. Pruden, Economics of thermal dissociation of H2S to produce hydrogen, Int. J. Hydrog. Energy 23 (7) (1998) 531–544.
[40] I. Traus, H. Suhr, Hydrogen sulfide dissociation in ozonizer discharges and operation of ozonizers at elevated temperatures, Plasma Chem. Plasma Process. 12 (3) (1992) 275–285.
[41] J.E. Nicholas, C.A. Amodio, M.J. Baker, Kinetics and mechanism of the decomposition of H 2 S, CH 3 SH and (CH 3) 2 S in a radio-frequency pulse discharge, Journal of the Chemical Society, Faraday Transactions 1: Physical Chemistry in Condensed Phases. 75 (1979) 1868–1875.
[42] J.B. Harkness, R.D. Doctor, E.J. Daniels, Plasma-chemical conversion of hydrogen sulfide into hydrogen and sulfur, Argonne National Lab., IL (United States), 1993.
[43] E. Krasheninnikov, V. Rusanov, S. Sanyuk, A. Fridman, Dissociation of hydrogen sulfide in an RF discharge, Zh Tekh Fiz. 56 (1986) 1104–1109.
[44] V. Dalaine, J. Cormier, S. Pellerin, P. Lefaucheux, H 2 S destruction in 50 Hz and 25 kHz gliding arc reactors, J. Appl. Phys. 84 (3) (1998) 1215–1221.
[45] V. Dalaine, J. Cormier, P. Lefaucheux, A gliding discharge applied to H 2 S destruction, J. Appl. Phys. 83 (5) (1998) 2435–2441.
[46] T. Nunnally, K. Gutsol, A. Rabinovich, A. Fridman, A. Gutsol, Plasma dissociation of H2S with O2 addition, Int. J. Hydrog. Energy 39 (24) (2014) 12480–12489.
[47] N. Tippayawong, E. Chaiya, P. Thanompongchart, P. Khongkrapan, Sustainable energy from biogas reforming in a microwave discharge reactor, Procedia Engineering. 118 (2015) 120–127.
[48] J.-L. Liu, X.-S. Li, X. Zhu, K. Li, C. Shi, A.-M. Zhu, Renewable and high-concentration syngas production from oxidative reforming of simulated biogas with low energy cost in a plasma shade, Chem. Eng. J. 234 (2013) 240–246.
[49] J.-L. Liu, H.-W. Park, W.-J. Chung, W.-S. Ahn, D.-W. Park, Simulated biogas oxidative reforming in AC-pulsed gliding arc discharge, Chem. Eng. J. 285 (2016) 243–251.
[50] X. Guofeng, D. Xinwei, Optimization geometries of a vortex gliding-arc reactor for partial oxidation of methane, Energy. 47 (1) (2012) 333–339.
[51] C.S. Kalra, Y.I. Cho, A. Gutsol, A. Fridman, T.S. Rufael, Gliding arc in tornado using a reverse vortex flow, Rev. Sci. Instrum. 76 (2) (2005) 025110.
[52] E. George, W.G. Hunter, J.S. Hunter, Statistics for experimenters: an introduction to design, data analysis, and model building: J, Wiley, 1978.
[53] A. Gutsol, A. Rabinovich, A. Fridman, Combustion-assisted plasma in fuel conversion, J. Phys. D. Appl. Phys. 44 (27) (2011) 274001.
[54] Z. Bo, S. Mao, Z.J. Han, K. Cen, J. Chen, K.K. Ostrikov, Emerging energy and environmental applications of vertically-oriented graphenes, Chem. Soc. Rev. 44 (8) (2015) 2108–2121.
[55] X.-H. Lin, J.-G. Gai, Synthesis and applications of large-area single-layer graphene, RSC Adv. 6 (22) (2016) 17818–17844.
[56] T. Hesjedal, Continuous roll-to-roll growth of graphene films by chemical vapor deposition, Appl. Phys. Lett. 98 (13) (2011) 133106.
[57] R. Varella, J. Sagás, C.J.F. Martins, Effects of plasma assisted combustion on pollutant emissions of a premixed flame of natural gas and air, 184 (2016), pp. 269–276.
[58] H.H. Nguyen, A. Nasonova, I.W. Nah, K.-S. Kim, Analysis on CO2 reforming of CH4 by corona discharge process for various process variables, J. Ind. Eng. Chem. 32 (2015) 58–62.
[59] S. Lu, L. Chen, C. Du, X. Sun, X. Li, J. Yan, Experimental study of hydrogen production from reforming of methane and ammonia assisted by Laval nozzle arc discharge, Int. J. Hydrog. Energy 39 (35) (2014) 19990–19999.
[60] B. Zhu, X.-S. Li, J.-L. Liu, A.-M. Zhu, Optimized mixed reforming of biogas with O2 addition in spark-discharge plasma, Chem. Eng. J. 37 (22) (2012) 16916–16924.
[61] N. Rueangjitt, T. Sreethawong, S. Chavadej, Reforming of CO 2-containing natural gas using an AC gliding arc system: effects of operational parameters and oxygen addition in feed, Plasma Chem. Plasma Process. 28 (1) (2008) 49–67.
[62] J.-L. Liu, H.-W. Park, W.-J. Chung, D.-W. Park, High-efficient conversion of CO 2 in AC-pulsed tornado gliding arc plasma, Plasma Chem. Plasma Process. 36 (2) (2016) 437–449.
[63] T.C. Chou, T.Y. Lin, B.J. Hwang, C.C. Wang, Selective removal of H2S from biogas by a packed silica gel adsorber tower, Biotechnol. Prog. 2 (4) (1986) 203–209.
[64] C.-Y. Lin, P.-H. Hesu, D.-H. Yang, Removal of hydrogen sulfide gas and landfill leachate treatment using coal bottom ash, Journal of the Air Waste Management Association. 51 (6) (2001) 939–945.
[65] D. Montes, E. Tocuyo, E. González, D. Rodríguez, R. Solano, R. Atencio, et al., Reactive H2S chemisorption on mesoporous silica molecular sieve-supported CuO or ZnO, Microporous Mesoporous Mater. 168 (2013) 111–120.
[66] P. Cherosky, Y. Li, Hydrogen sulfide removal from biogas by bio-based iron sponge, Biosyst. Eng. 114 (1) (2013) 55–59.
[67] D. Mescia, S. Hernández, A. Conoci, N. Russo, MSW landfill biogas desulfurization, Int. J. Hydrog. Energy 36 (13) (2011) 7884–7890.
[68] K. Jones, A. Martinez, M. Rizwan, J. Boswell, Sulfur toxicity and media capacity for H2S removal in biofilters packed with a natural or a commercial granular medium, Journal of the Air Waste Management Association. 55 (4) (2005) 415–420.
[69] S. John, J.C. Hamann, S.S. Muknahallipatna, S. Legowski, J.F. Ackerman, M.D. Argyle, Energy efficiency of hydrogen sulfide decomposition in a pulsed corona discharge reactor, Chem. Eng. Sci. 64 (23) (2009) 4826–4834.
[70] E.L. Reddy, V. Biju, C. Subrahmanyam, Production of hydrogen from hydrogen sulfide assisted by dielectric barrier discharge, Int. J. Hydrog. Energy 37 (3) (2012) 2204–2209.
[71] I. Traus, H. Suhr, J. Harry, D. Evans, Application of a rotating high-pressure glow discharge for the dissociation of hydrogen sulfide, Plasma Chem. Plasma Process. 13 (1) (1993) 77–91.